Wood Science and Technology (2025) 59:21
https://doi.org/10.1007/s00226-024-01624-4

ORIGINAL

Lignin hygroexpansion in compression and opposite wood - a molecular dynamics study

Marie Hartwig-Nair[1] · Alexandr Nasedkin[1] · Klara Hackenstrass[1] · Emiliano De Santis[2] · Sara Florisson[1] · Malin Wohlert[1]

Received: 19 June 2024 / Accepted: 30 November 2024
© The Author(s) 2024

Abstract

Softwood branches develop compression wood (CW) in the lower parts of the branch, while opposite wood (OW) develops on the upper. These wood types differ in structure at several length scales, among others in the chemical composition of their lignin matrix. While OW mostly contains guaiacyl (G) units, CW is known to contain a substantial fraction of 4-hydroxyphenyl (H) lignin. In this study, the impact this difference has on lignin hygroexpansion and interaction with water is studied by the means of atomistic models and molecular dynamics computer simulations of lignin systems at different levels of hydration. It was found that, despite the minor difference in chemical composition, there are differences in swelling, structure and water dynamics. CW lignin is found to have a higher uniaxial swelling coefficient, since the phase separation between lignin and water is more pronounced. This behavior is linked to structural differences, where intermolecular $\pi - \pi$ stacking is more common in CW lignin and hydrogen bonding to water more pronounced in OW lignin. These findings are of interest for understanding the role of lignin in CW, and general understanding of moisture interaction with lignin inside wood cell walls.

Introduction

In softwood trees, such as spruce, nearly 20 % of the biomass is wood that originates from branches (He et al. 2018). Within softwood branches, reaction wood called compression wood (CW) is found, with macro- and microscopic properties that are different from the opposite wood (OW) found mirrored to the CW within the cross section of a branch or the normal wood (NW) from the trunk. The branches are usually left as waste or used as firewood. From a sustainability perspective, the creation of products also from secondary wood resources is a high priority. The key to better use of this material is to better understand the connection between its structural features and properties.

Marie Hartwig-Nair and Alexandr Nasedkin are first authors.

Extended author information available on the last page of the article

Published online: 23 December 2024

Wood is a hierarchical material, where the softwood microstructure is traditionally described with characteristic cross-section length scales such as (Gibson 2012; Wohlert et al. 2022):

- tracheids (20 μm)
- cell walls (1 μm)
- cell wall layers (0.1 μm)
- fibril aggregates (10 – 100 nm)
- cellulose fibrils (5 nm)
- individual wood polymers (may be μm long but $<$ 1 nm cross section)

Branch CW is known to differ from OW and NW on several of these length scales. The cross sections of CW tracheids are circular rather than hexagonal with thicker cell walls. CW cell walls also lack the S3 layer and have a higher microfibril angle in the S2 layer (Gardiner et al. 2014b; Hartwig-Nair et al. 2024a, b). Furthermore, CW contains less cellulose and more lignin with a higher ratio of 4-hydroxyphenyl (H) as compared to guaiacyl (G) units. Lignin in CW is also homogeneously distributed throughout the S2 layer, while mainly located in the middle lamella of OW (Färber et al. 2001; Timell 1986; Donaldson et al. 2016; Gardiner et al. 2014a; Li et al. 2014; Zhang et al. 2016). These differences in chemical composition and cell wall characteristics are likely to affect both mechanical and hygroexpansion properties, which have been scarcely investigated (Timell 1986; Gurau et al. 2008; Harris 1977; Perstorper et al. 2001; Burgert et al. 2004; Müller et al. 2006; Stanzl-Tschegg et al. 2011; Hartwig-Nair et al. 2024a).

The interaction between wood and moisture is crucial for a living tree and challenging for the engineering use of wood, since it gives rise to distortion and cracking. When moisture level is below the fibre saturation point, changes in relative humidity can induce dimensional changes of the wood structure. For stem NW, the changes in longitudinal direction are usually small (swelling coefficient 0.006), while the radial and tangential swelling is larger (0.16 – 0.33) (Bengtsson 2001). Wood that contains both CW and NW/OW is known to develop internal stresses due to differential swelling, especially in the longitudinal direction. In a recent study, swelling coefficients were determined in longitudinal direction of CW to be 0.246 at 75 % relative humidity, while swelling coefficients in transverse directions were in the same order of magnitude as for OW (Hartwig-Nair et al. 2024a). The explanation for CW to have a substantially larger longitudinal swelling coefficient has been attributed to its large microfibril angle (Färber et al. 2001). However, it has also been suggested that other polymers such as lignin and highly hygroscopic (1$\longrightarrow$3)-β-D-glucans make an impact on the swelling behavior and not to forget the previously mentioned differences in lignin distribution within the cell wall of CW and NW (Leonardon et al. 2010).

Molecular-scale interaction between water and lignin in wood cell walls are not fully understood, despite their crucial role in applications of biomass. Molecular modeling such as with molecular dynamics (MD) simulations can provide detailed insights into molecular-scale phenomena. This method is frequently applied to cellulose, and to some extent to hemicellulose and lignin. The method surpasses what

can be reached by experimental methods and the method also has the ability to quantitatively extract almost any experimental parameter from the simulated ensemble (Wohlert et al. 2022; Paajanen et al. 2022; Kulasinski et al. 2015; Zitting et al. 2023). Nevertheless, the connection between microscopic molecular properties and macroscopic phenomena is not always clear, and ultimately multi-scale approaches are needed to fully describe properties like wood swelling.

At the molecular scale, a living wood cell wall is a hydrated tissue that can be described as a polymer nanocomposite with stiff cellulose nanofibrils embedded in a polymer matrix. The cellulose crystalline cores are inaccessible to water, embedded in (hydrated) hemicellulose and glued by (hydrated) lignin. The simple but widely used model proposed in the 70's by Fengel (Fengel 1971) shows square fibril aggregates with hemicellulose between cellulose and lignin outside. However, this model might provide a somewhat too simplified picture. Recent findings with electron tomography unraveled for instance a highly complex structure inside the cell wall (Fernando et al. 2023). The study showed extended cellulose fibrils and fibril aggregates in combination with hemicellulose, lignin and nanopores. Predicting swelling of wood cell walls by considering its molecular structure is therefore challenging. Molecular dynamics (MD) simulations have been applied to address the swelling, on a cell wall level (Kulasinski et al. 2015; Zhang et al. 2021), combined with X-ray scattering techniques (Paajanen et al. 2022) and to show that water is needed to thermodynamically stabilize cellulose fibril aggregates (Chen et al. 2022). In brief, changing the surrounding moisture conditions will affect the structural arrangement of wood polymers. When it comes to CW, its swelling properties due to high microfibril angle was investigated by micromechanic modeling, supporting its overall importance (Joffre et al. 2014).

The aim of this study is to investigate the importance of the lignin chemical structure for the swelling differences seen in CW by studying lignin of different composition (pure G lignin and G/H lignin) under various moisture conditions with MD simulations. Throughout this paper, two lignin models are in focus. One represents CW lignin and is denoted GGGH, while the other representing OW/NW lignin is denoted GGGG, indicating their chemical composition.

Methods

The present study uses atomistic models and MD simulations to investigate lignin hygroexpansion. This section therefore contains details of the different simulated systems as well as input parameters for the simulation protocols and details about the analysis.

Molecular topology

Lignin in CW and OW is in the present study represented as a system of 1000 all β-O-4' linked tetramers. Their molecular structures are displayed in Fig. 1. Opposite wood lignin is represented by an all-guaiyacyl (GGGG) tetramer, with four β-O-4'

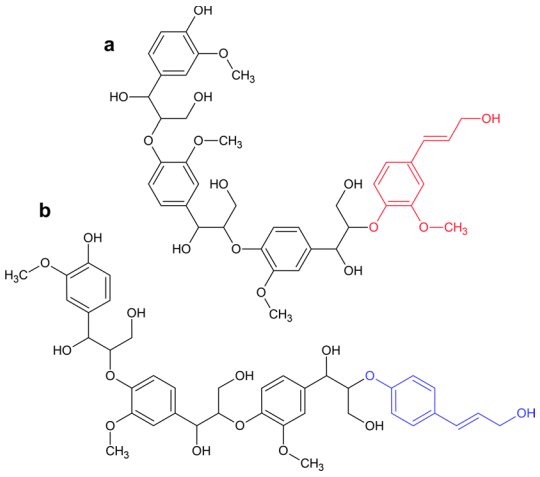

Fig. 1 Lignin model tetramers: a) a GGGG (OW/NW) tetramer and b) a GGGH (CW) tetramer. The only difference between the two molecules is the presence of an extra methoxy group at the last monomer that is highlighted in red or blue

linked G (coniferyl) units. In the compression wood lignin model, one of the G units is exchanged by an H (4-hydroxyphenyl) unit, denoted GGGH tetramer. CHARMM force field for lignin (Vermaas et al. 2019) and the TIP3P model for water (Jorgensen et al. 1983) were used. The lignin topology was transformed with the TopoTools plugin (Vermaas et al. 2016) for VMD (Humphrey et al. 1996).

System setup

Boxes with 1000 lignin molecules of either GGGG and GGGH type were prepared by inserting lignin molecules into an empty box withthe GROMACS 2019.6 (Abraham et al. 2015; Páll et al. 2015) program `gmx insert-molecules` and filled with water to 20 different levels of moisture content (MC) ranging between 0.1 and 0.26. The initial size of the box was set to 15.5 nm for either 1000 lignin tetramers of type GGGG or GGGH. This setting provides enough room to accommodate the large volume of water as well. A number of water molecules were inserted into the box of lignin to achieve the desired level of hydration. The exact number of added water is tabulated in Table 1, and an example of a simulation box at 10 % MC is shown in Fig. 2.

Simulation protocol

The MD simulations and consecutive analysis of trajectories were run in with GROMACS 2019.6 (Abraham et al. 2015; Páll et al. 2015). In total, 40 different simulations were performed according to the same protocol. To avoid initial position clashes or the atoms, energy minimization of the system is needed prior to the dynamic MD simulation. The prepared systems were subjected to energy minimization for a maximum of 10000 steps with the steepest descent algorithm. Energy minimized structures were further exerted to simulated annealing to

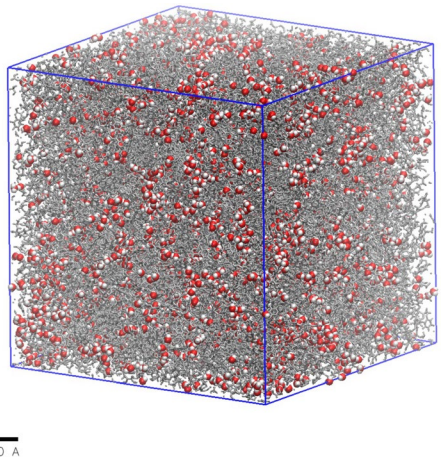

Fig. 2 Illustration of one simulation box. Snapshot of a GGGG box at 10 % MC. Lignin molecules are depicted in licorice representation and coloured in grey and water molecules using the Van der Waals spherical representation of the atoms

Table 1 Number of water molecules and corresponding moisture content in lignin/water systems

System ID	Number of water molecules	Moisture content [%]	
		a:GGGG	b:GGGH
1a/1b	**430**	**1.01**	**1.05**
2a/2b	**870**	**2.04**	**2.12**
3a/3b	**1320**	**3.09**	**3.22**
4a/4b	**1780**	**4.17**	**4.34**
5a/5b	**2250**	**5.27**	**5.49**
6a/6b	**2720**	**6.38**	**6.63**
7a/7b	**3210**	**7.52**	**7.83**
8a/8b	**3710**	**8.70**	**9.05**
9a/9b	4220	9.89	10.29
10a/10b	4740	11.11	11.56
11a/11b	5270	12.35	12.85
12a/12b	5820	13.64	14.20
13a/13b	6380	14.95	15.56
14a/14b	6950	16.29	16.95
15a/15b	7530	17.65	18.37
16a/16b	8130	19.05	19.83
17a/17b	8740	20.48	21.32
18a/18b	9370	21.96	22.85
19a/19b	10010	23.46	24.41
20a/20b	10670	25.01	26.02

The molecular weights are 768 g/mol and 738 g/mol for GGGG and GGGH tetramers respectively. The number of lignin tetramers is 1000 for every system. Systems shaded in bold are analyzed for swelling only

ensure proper equilibration. The heating cycle was designed to allow lignin to overcome possible energetic barriers and to sample all available configurations. The temperature was set to 10 K during the first nanosecond of simulation, and then linearly increased to 500 K during the next 9 ns, kept constant for one more nanosecond and decreased linearly from 500 K to 300 K during the following 9 ns (Fig. 3). Afterwards, every system was simulated in an NPT ensemble under constant temperature and pressure for another 100 ns, of which the first half is considered an equilibration and the last 50 ns were used in the analysis.

The temperature and pressure were controlled by coupling to an external bath with a velocity-rescale thermostat (Bussi et al. 2007) and a Berendsen barostat (Berendsen et al. 1984), respectively. Time constants were 0.1 ps and 2 ps for temperature and pressure, respectively. The compressibility of the system was set to $4.5 \cdot 10^{-5}$ bar^{-1} and the pressure to 1 bar. Short-range non-bonded interactions (both electrostatic and van der Waals) were treated explicitly with a cut-off radius of 1.4 nm. Long-range electrostatic interactionss between atoms were accounted for by the Particle Mesh Ewald algorithm (Darden et al. 1993), the default Potential-Shift-Verlet modifier was used for electrostatic and van der Waals interactions. Newton's second equation of motion was integrated with the Leap-Frog algorithm (Hockney et al. 1974; Berendsen and van Gunsteren 1986). The integration time-step was 1 fs and the atomic coordinates were recorded every 5 ps. No atomic position constraints were applied.

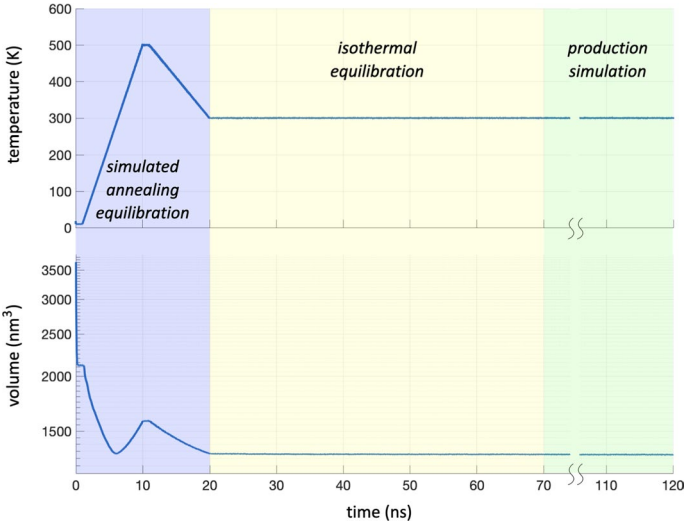

Fig. 3 Example of temperature and volume variation in the MD run. Intervals for temperature varying simulated annealing equilibration, constant temperature equilibration and production MD run used for analysis are highlighted in blue, yellow and green, respectively

Analysis

Mass-weighted radius of gyration R_g was calculated with the GROMACS gmx gyrate analysis tool (Abraham et al. 2015; Páll et al. 2015) as

$$R_g^2 = \frac{1}{M}\sum_{i=1}^{N} m_i(\bar{r}_i - \bar{R})^2 \tag{1}$$

where $M = \sum_{i=1}^{N} m_i$ is the total mass of a molecule and $\bar{R} = \frac{1}{N}\sum_{i=1}^{N} \bar{r}_i$ is the center of mass of the molecule consisting of N atoms.

The occurrence of two key structural arrangements, namely $\pi - \pi$ sandwich and T-shaped $\pi - \pi$ arrangements, among lignin molecules is investigated. To quantify these arrangements, a custom Python script utilizing the MDAnalysis library (Michaud-Agrawal et al. 2011) was developed. Similarly to previous studies (Ribca et al. 2023), $\pi - \pi$ sandwich stacking is defined by the proximity of aromatic rings, indicated by a distance between their planes less than 0.5 nm, along with an angle between the ring planes in the range of 180° ± 20°. On the other hand, T-shaped $\pi - \pi$ arrangements are identified when the distance between the ring planes falls between 0.55 nm and 0.72 nm, with their respective angles lying within 70° to 110°. To ensure statistical robustness, the occurrences of both $\pi - \pi$ sandwich and T-shaped $\pi - \pi$ stacking are assessed and averaged, with evaluations conducted at 5 ns intervals over the final 50 ns of equilibrated simulations across varying MC conditions. The contributions of intermolecular and intramolecular stacking are analyzed independently and the averaged numbers are normalized with respect to number of lignin molecules (1000).

Hydrogen bonds were detected by geometric criteria using the GROMACS `gmx hbond` tool (Abraham et al. 2015; Páll et al. 2015), with a cutoff donor-acceptor distance of 0.35 nm and a cutoff angle of 30°.

Radial distribution functions were calculated with the `gmx rdf` tool according to Equation 2, where $\langle \rho_B(r) \rangle$ is the particle density of type B at a distance r around particles A, and $\langle \rho_B \rangle_{local}$ is the particle density of type B averaged over all spheres around particles A with radius r_{max}.

$$g_{AB}(r) = \frac{\langle \rho_B(r) \rangle}{\langle \rho_B \rangle_{local}} \tag{2}$$

Water density maps were produced by averaging over the last 50 ns of the simulations, using the MDAnalysis toolkit and the MDAnalysis.analysis.density function (Michaud-Agrawal et al. 2011) with a bin size of 1.0 Å. As a measure to quantify differences in water density distribution, the root mean square roughness (R_q) was calculated based on water density values in each point (ρ_i) and their deviation from mean density ($\bar{\rho}$) according to Eq. 3.

$$R_q = \sqrt{\frac{1}{N}\sum_{i=1}^{N} (\rho_i - \bar{\rho})^2} \tag{3}$$

Linear regression and statistical analysis was performed with MATLAB (Inc 2024). Analysis of variance (ANOVA) was performed using the `anova` function. This function provided statistical estimates and significance testing.

Results and discussion

Volumetric and uniaxial expansion

The average box volume at different MC is shown in the first graph in Fig. 4 together with the volume expansion, V, with respect to the initial box volume with no water, V_0 visualised in the second graph of Fig. 4. The first graph in Fig. 4 suggests the presence of two regions with different swelling behavior based on the shape of the curve. Below a MC of 0.1, swelling is slower, indicating water primarily entering empty spaces in the lignin matrix. At higher MC, the swelling rate is increased, pushing the lignin matrix apart. The second graph in Fig. 4 also shows the theoretical limit of expansion, i.e. the volume increase due to added water, assuming the volume of one water molecule to be 0.03 nm^3. All simulations show a volume expansion less than the theoretical limit, suggesting a mixing between lignin and water. This can be seen as water filling the pores and cavities in the box of lignin without forming large clusters of bulk water.

The subsequent analysis in this paper will focus on the swelling behavior, structure and dynamics of lignin and water in the second regime between a MC of 0.1 and 0.3, where 0.3 is close to the fibre saturation point of wood. This means that in the following sections, results from simulations $9-20$ in Table 1 will be presented.

In Fig. 5, the uniaxial expansion is shown determined as the cube root of volume expansion, assuming isotropic swelling. To enhance visibility of the differences between the two lignin systems, a baseline is subtracted, corresponding to a straight line with slope equal to 0.3. The GGGG and GGGH uniaxial expansion data in this region was fitted to a linear function for estimating the uniaxial expansion coefficients β_{GGGG} and β_{GGGH}, respectively. These are also presented in Fig. 5. It is noted

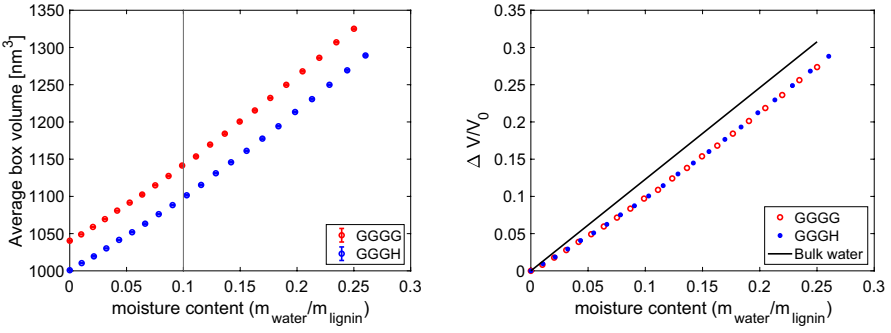

Fig. 4 Absolute box volume versus moisture content (left) and volume expansion versus moisture content (right)

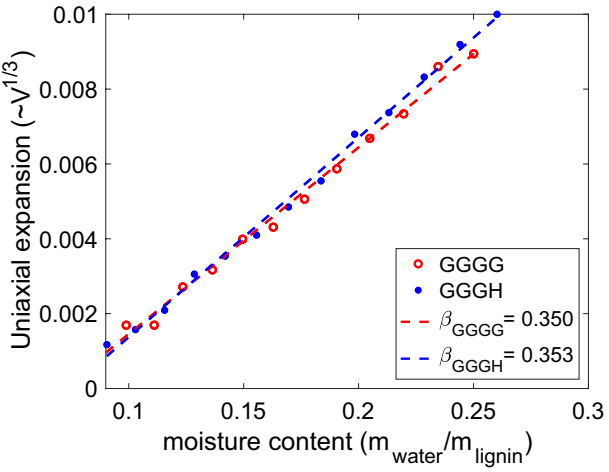

Fig. 5 Uniaxial expansion epsilon of the simulation box upon addition of water. The system comprising GGGG tetramers (opposite wood) shows higher expansion coefficient compared to the GGGH tetramers (compression wood). An ANOVA test provided a nonlinear p-value of 0.042, suggesting a significant difference between the coefficients

that there is only a small but significant (p-value less than 0.05) difference in uniaxial hygroexpansion coefficients between the two systems, where GGGH lignin has a higher expansion coefficient. Given that the only difference in chemical structure is the presence of an extra methoxy group on each GGGG tetramer, it is still remarkable that such a minor structural difference gives rise to a different swelling behavior for a lignin matrix system.

Lignin structure

To find explanations for the different swelling properties of GGGG and GGGH lignin, the lignin structure is analyzed in detail.

Radius of gyration

In brief, radius of gyration, R_g, provides information about the compactness of each lignin molecule. In Fig. 6, average values of R_g are presented. For the GGGG lignin, results for both the entire tetramer and with its extra methoxy group omitted are presented. The data show that GGGH lignin is on average more compact at all levels of moisture content, but also that its R_g decreases more significantly than GGGG as moisture content increases. It is also clear that the observed dissimilarities in R_g between GGGG and GGGH are due to conformation differences and not the fact that GGGG is larger in size. It has previously been shown that single GG-dimers in water linked by β-O-4' linkage are prone to adapt a folded conformation, and that lower R_g is a consequence of folding (Hackenstrass et al. 2024).

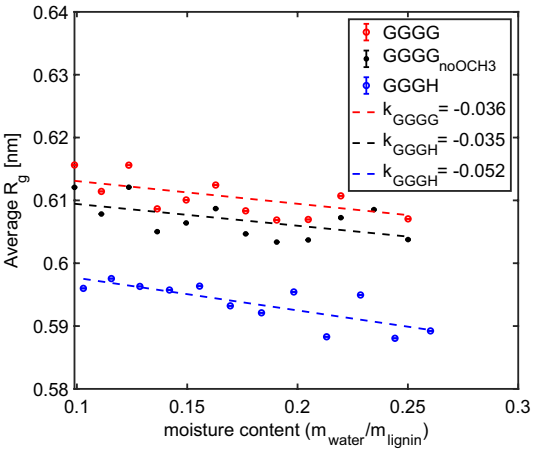

Fig. 6 Average values of R_g at different moisture content with fitted trend lines. For GGGG, results are shown for both entire tetramer and with its extra methoxy group omitted. The *k*-values in the legend indicate slope gradient. Error bars are included but smaller than the markers. An ANOVA test provided a nonlinear p-value of 0.045, suggesting a significant difference between the GGGG and GGGH coefficients

The lower average R_g and the more pronounced decrease in R_g with increasing MC for GGGH tetramers therefore suggests more folded lignin compared to GGGG, although the molecule is somewhat smaller already from the beginning, due to the extra hydroxymethyl group on GGGG. It also shows that increased MC affects GGGH more than GGGG conformation. Snapshots from GGGG and GGGH simulations in Fig. 7 illustrate examples of folded and unfolded conformations of the two tetramers. In stretched conformation, the presence of an extra methoxy group at the GGGG lignin molecule does not affect conformation, whereas folded, the GGGH is able to turn into a more compact shape due to its smaller size. It is worth noting that the example conformations shown in Fig. 7 are snapshots only and that it is the statistically obtained R_g data that is important. Other stretched or folded conformations than the ones shown in Fig. 7 may occur, but on visual inspection of the trajectories, no occurrence of the compact shape was seen in the GGGG system.

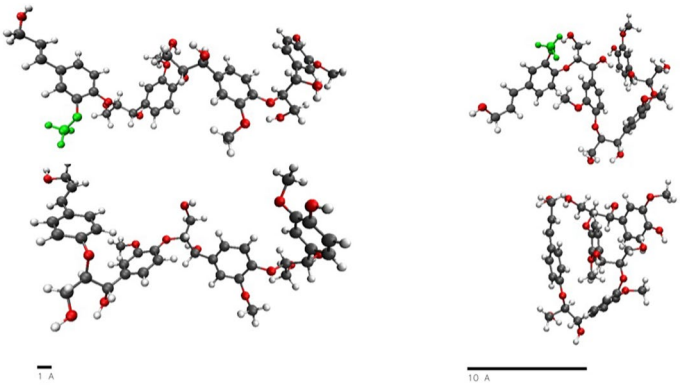

Fig. 7 Stretched and folded conformations of GGGG (top) and GGGH (bottom) in MC=0.25. The additional methoxy group in GGGG is highlighted in green

Given that swelling is more pronounced for the GGGH system, the difference is not due to individual lignin molecules taking up more space, but rather an increased distance between the molecules.

Lignin $\pi - \pi$ stacking

Figure 8 presents the occurrence of $\pi - \pi$ stacking arrangements per lignin molecule as a function of the MC in the different simulations as detected by geometric criteria described in the methods section. The top panels show T-shaped and the bottom panels sandwich-shaped $\pi - \pi$ stacking. In both panels the results from intra- and intermolecular arrangements are separated.

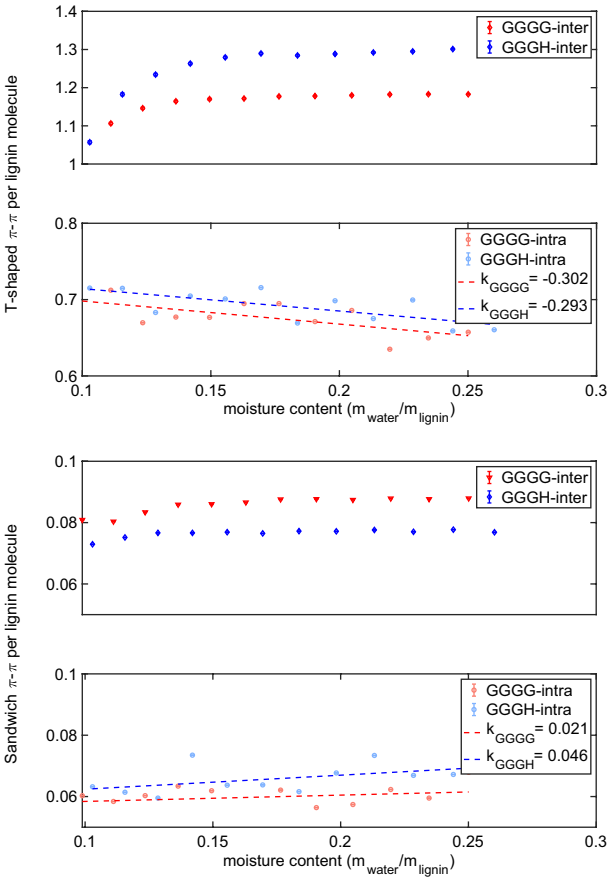

Fig. 8 In the top panels, the average number of T-shaped $\pi - \pi$ stacking arrangements per lignin molecule is presented, while the bottom panels showcase the average number of sandwich $\pi - \pi$ stacking per lignin molecule. In each panel, the results for intermolecular stacking and intramolecular stacking are shown separately. For intramolecular data, fitted trend lines with increasing moisture content are shown. An ANOVA test yielded a nonlinear p-value of 0.9 for the T-shaped figure and 0.5 for the sandwich-shaped one, indicating no statistically significant differences between the slopes

It is clear from the figure that T-shaped $\pi - \pi$ stacking is more common than sandwich-shaped, and that intermolecular $\pi - \pi$ stacking is more common than intramolecular. Notably, subtle differences between GGGG and GGGH are observed. T-shaped stacking is more common in the GGGH tetramer compared to GGGG. On the contrary, although more rarely occuring than T-shaped, the GGGG tetramer exhibits a higher occurrence of sandwich-shaped stacking.

Considering the variation with increasing MC, the intermolecular stacking reaches plateau values after initial increase. For T-shaped stacking, GGGH tetramer reaches its plateau at higher concentrations compared to the GGGG tetramer. Conversely, for sandwich stacking, the plateau value is reached at lower MC levels for the GGGH tetramer.

However, the results of intramolecular $\pi - \pi$ arrangements is less conclusive. There appears to be an negligible increasing dependency on MC for sandwich-shaped, while T-shaped contributions exhibit a decreasing trend as the MC values increase. The dependence was analyzed by a linear fit, and an ANOVA test yielded a nonlinear p-value of 0.9 for the T-shaped fitted line and 0.5 for the sandwich line, indicating no statistically significant differences between the slopes in any of them.

Hydrogen bonds

In addition to lignin $\pi - \pi$ stacking, hydrogen bonds (HB) between lignin-lignin and lignin-water may stabilize certain conformations, due to them being energetically favorable. The average number of hydrogen bonds between lignin-lignin (both intra- and intermolecular) and between water-lignin were therefore calculated, and the results are presented in Fig. 9. The average number of lignin-lignin hydrogen bonds is similar in the two systems and decreasing with increasing MC. On the other hand, the additional methoxy group on GGGG lignin provides an extra opportunity for water to form hydrogen bonds to this lignin type. The average number of hydrogen bonds between GGGG and water GGGH and water increases with increasing MC. At MC 0.1, the average number of lignin-water HB per lignin molecule is similar,

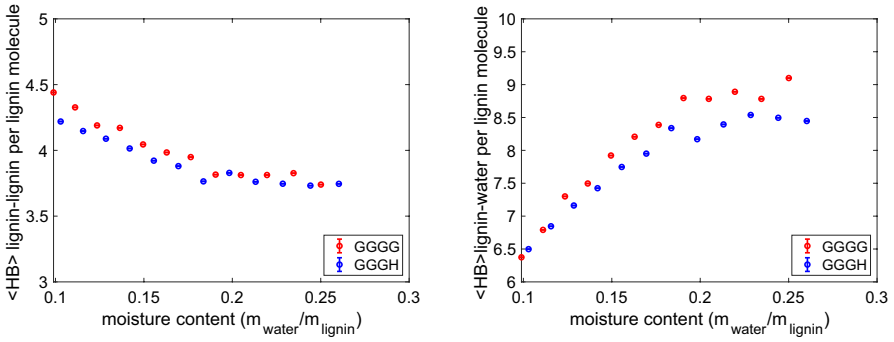

Fig. 9 Average number of hydrogen bonds (HB:s) - lignin-lignin (left) and lignin-water (right). The numbers are normalized with respect to number of lignin molecules (1000)

around 6.5. However, at the highest MC around 0.3, there is a difference between the two systems. The average number of HB per GGGG molecule and water increases to about 9 whereas between GGGH and water the increase is less significant, to about 8.5 HB per lignin molecule.

Water structure

To investigate the water distribution in the two lignin matrices, an averaged 2D-density map of water at different levels of MC normalized to water bulk density is presented for both systems in Fig. 10. In both systems, water at low MC is homogeneously distributed over the matrix, filling the spaces between lignin molecules that become hydrated. As MC increases, a difference between the two systems appears, where water seems more homogeneously distributed in the GGGG system compared to GGGH with deeper valleys indicating areas where water is depleted. Nevertheless, water clusters with a density value of bulk water are visible in both systems. As the difference is challenging to discern visually, supplementary calculations were performed to quantify the water density landscape in the two systems as described in the methods section. The results are presented in Table 2 and the higher roughness of GGGH density maps at high MC support the visual impression that water is more homogeneously distributed in the GGGG lignin matrix.

To further investigate the water structure around lignin molecules, radial distribution functions (RDF) of water with respect to different functional groups are presented in Fig. 11. RDF provides the probability of finding a water molecule at a certain distance from the different functional groups. The definition of functional groups is found in SI Figure SI-1. It is clear, and not surprising, that water prefers to be close and ordered (sharp peaks at small r) around hydroxy and methoxy groups while it avoids the aromatic rings. Linkages and alkyl groups seem to have more water close to them at low MC than at high MC. The main difference between GGGG and GGGH is that water is depleted especially from the alkyl groups in GGGH at higher MC.

In addition, center-of-mass RDF:s were calculated between lignin-lignin and lignin-water at high moisture content (MC= 0.25). The results are presented in Fig. 12 to visualize the total structure.

Center-of-mass RDF:s of oligomer molecules are difficult to interpret due to the flexibility of the chain leading to diffuse RDF:s without well-defined peaks. However, a hydration layer is found closer than COM distance between first lignin neighbors. Relative coordination numbers of lignin and water calculated according to Eq. 4 using unit number density ρ and $r_{max} = 1.5$ nm for lignin-lignin and

Table 2 Root mean square roughness (R_q, dimensionless) of the water density maps shown in Fig. 10 according to Eq. 3

	MC 0.1	MC 0.15	MC 0.2	MC 0.25
GGGG	0.078	0.086	0.113	0.152
GGGH	0.079	0.096	0.142	0.165

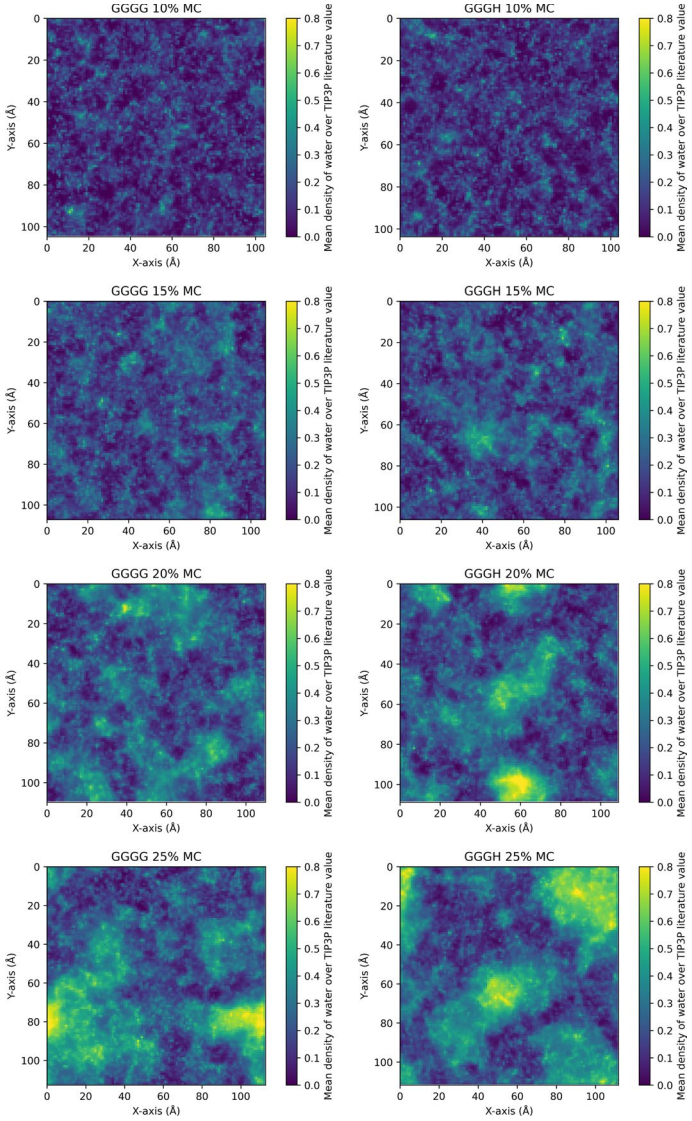

Fig. 10 Average water density maps at MC 0.1, 0.15, 0.2 and 0.25. Corresponding surface roughness is presented in Table 2

$r_{max} = 1$ nm for lignin-water are presented in Table 3 indicating closer packing of GGGH lignin and more hydrated GGGG lignin in concordance with other structural analysis.

$$CN = 4\pi\rho \int_0^{r_{max}} r^2 g(r) dr \tag{4}$$

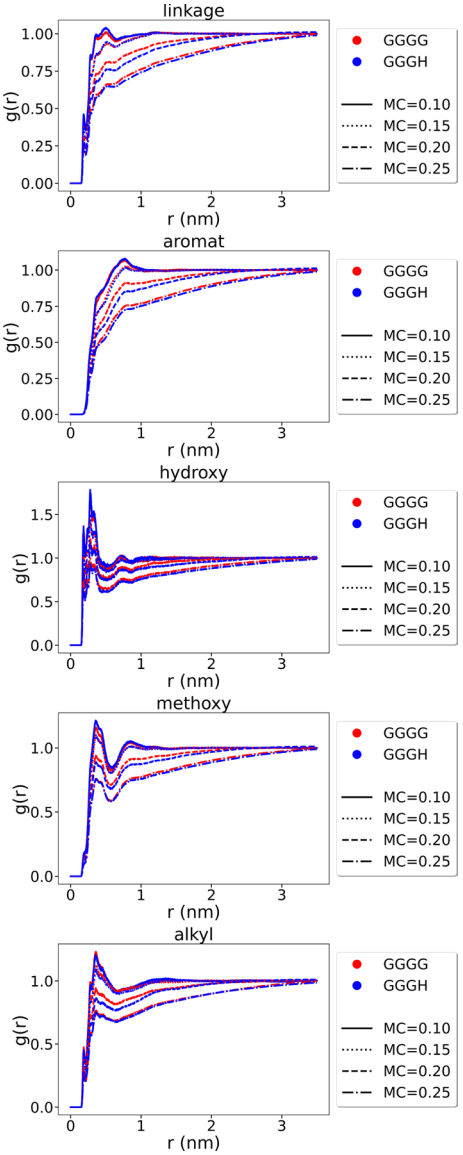

Fig. 11 Radial distribution functions (RDF:s) of water around lignin functional groups (definition of groups in Figure SI-1) at four different levels of MC (0.1−0.25)

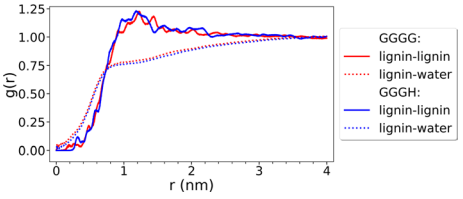

Fig. 12 Lignin-lignin and lignin-water RDF:s at MC=0.25

Table 3 Relative coordination numbers (CN) at MC=0.25 calculated from the RDF:s in Figure 12 according to Eq. 4

	Lignin-lignin CN	Lignin-water CN
GGGG	14.35	2.75
GGGH	14.42	2.68

Table 4 Main differences between GGGG and GGGH simulations

Property	GGGG (OW)	GGGH (CW)
Hygroexpansion	Less	More
Radius of gyration	Larger	Smaller
Intermolecular $\pi - \pi$	Less	More
HB to water	More	Less
Water density	More homogeneous	Less homogeneous
Water diffusion	Slower	Faster

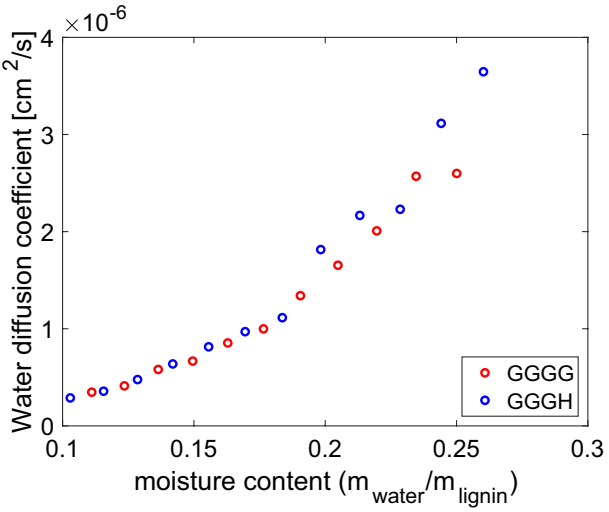

Fig. 13 Water diffusion coefficients calculated from MSD. See Figure SI-2 for fitted trend lines

Water dynamics

Not only structure, but also dynamics of water was analyzed in the two lignin systems. The results are presented as translational diffusion constants calculated from mean square displacement (MSD) of water in the different simulations. The results are presented in Fig. 13. The water in the two systems is diffusing much slower than bulk water (the present TIP3P water model has a bulk self diffusion coefficient of $5.19 \cdot 10^{-5}$ cm^2s^{-1} Kumar et al. (2015)). Moreover, water diffusion in these lignin systems seem to have two regimes - one slower with a breaking point around MC 0.18 and one faster at MC above 0.18. In SI Figure SI-2 trend lines are fitted to the

data in each regime, showing that the difference between GGGG and GGGH water diffusion is significant only at higher MC where water diffuses slower in the GGGG system than in the GGGH system. In the GGGH system, water is more prone to form clusters and may diffuse faster. Water molecules that are confined in the lignin matrix are less mobile.

As a summary, all major differences are summarized in Table 4.

Conclusion

In this study, interaction between water and two different lignin models of idealized lignin matrices corresponding to opposite wood (GGGG) and compression wood (GGGH) was studied with molecular dynamics simulations. It was found that, despite the minor difference in chemical composition (GGGG lignin possessing an additional methoxy group), there are differences in swelling, structure and water dynamics. GGGH lignin is found to have a higher uniaxial swelling coefficient, although the difference is small (approximately 1 %). Lignin structural differences are identified. T-shaped $\pi - \pi$ stacking motifs are more common in both systems compared to sandwich-shaped, and occur more often in GGGH lignin. Sandwich $\pi - \pi$ stacking is generally less frequent but more common in GGGG lignin. The distribution of water also differs. The compression wood GGGH lignin forms more compact lignin clusters, while water is more homogeneously distributed in the GGGG lignin matrix. As a consequence, water dynamics is faster in the GGGH lignin matrix, since water is more confined inside the GGGG matrix.

The experimentally reported swelling differences of OW and CW tissue clearly show that these wood types differ in swelling, especially in the longitudinal direction where CW has a swelling coefficient more than ten times larger than OW. Can this difference be partially explained by the different swelling ability of OW and CW lignin? The simulation results in this study point to a small, yet significant, difference, but the question whether it explains tissue level swelling behavior of CW and OW or not remains unanswered.

One reason for the inability of such a molecular model to provide a full explanation is that the OW/CW differences span over several hierarchical levels (such as cell geometry, microfibril angle and cell wall layer morphology). Moreover, it is known that lignin content in CW is higher and differently distributed compared to OW, which may give the small difference in lignin swelling coefficient a larger impact. The present study contributes with molecular level understanding of lignin swelling mechanisms, but is not sufficient to explain its relative importance in this context.

Another reason is the simplified lignin models as perfectly monodisperse tetramers applied in the present study. Within the branches, lignin will have a variety of molecular weights, contain other linkages, and functional groups, and may also be covalently bonded to hemicelluloses as lignin-carbohydrate complexes (LCC), which would likely affect its swelling properties. What effect all these other differences contribute to the total swelling behavior of compression and opposite wood remains to be clarified.

However, the results presented in this study are of interest for future studies of wood swelling in general and the difference between CW and OW in particular. The main message is that, instead of considering lignin as a hydration-independent space filler, the findings presented here suggest that small variations in lignin chemistry can significantly influence its interaction with water and thereby macroscopic properties such as volumetric swelling or hygromechanical response.

In a future study, the mechanisms at different hierarchical levels could be addressed by a multiscale modeling approach, where the variation in lignin swelling properties at molecular scale can be taken into account and its relative importance for total tissue swelling can thereby be further elucidated. Although experimental investigation of CW/OW lignin swelling presents significant challenges, it remains of considerable interest. Techniques such as X-ray or neutron scattering offer potential avenues for such studies.

Supplementary Information The online version contains supplementary material available at https://doi.org/10.1007/s00226-024-01624-4.

Acknowledgements The authors acknowledge Prof. Kristofer Gamstedt for valuable discussions and Nil Tabudlong Jonasson for additional work with the stacking analysis.

Author contributions Conceptualization: Alexandr Nasedkin (AN), Marie Hartwig-Nair (MH), Klara Hackenstrass (KH), Sara Florisson (SF), Malin Wohlert (MW), Emiliano De Santis (EDS); Simulations: AN, KH, MW; Validation: AN, MW; Formal analysis and investigation: AN, MW, EDS; Writing—original draft: AN, MW; Writing—review & editing: MH, SF,EDS,KH; Visualization: MW; Supervision: MW, SF; Project administration: MW.

Funding Open access funding provided by Uppsala University.

Data availability All research data is stored on local computer cluster at Uppsala University.

Declarations

Conflict of interest The authors declare no conflict of interest.

Open Access This article is licensed under a Creative Commons Attribution 4.0 International License, which permits use, sharing, adaptation, distribution and reproduction in any medium or format, as long as you give appropriate credit to the original author(s) and the source, provide a link to the Creative Commons licence, and indicate if changes were made. The images or other third party material in this article are included in the article's Creative Commons licence, unless indicated otherwise in a credit line to the material. If material is not included in the article's Creative Commons licence and your intended use is not permitted by statutory regulation or exceeds the permitted use, you will need to obtain permission directly from the copyright holder. To view a copy of this licence, visit http://creativecommons.org/licenses/by/4.0/.

References

Abraham MJ, Murtola T, Schulz R et al (2015) Gromacs: high performance molecular simulations through multi-level parallelism from laptops to supercomputers. SoftwareX 1–2:19–25. https://doi.org/10.1016/j.softx.2015.06.001

Bengtsson C (2001) Variation of moisture induced movementsin Norway spruce (Picea abies). Ann For Sci 58(5):568–581. https://doi.org/10.1051/forest:2001146

Berendsen H, van Gunsteren W (1986) Practical algorithms for dynamics simulations. In: Molecular-Dynamics Simulations of Statistical-Mechanical Systems. Enrico Fermi Summer School, Soc. Italiana di Fisica, Varenna, Italy, p 43–65

Berendsen HJC, Postma JPM, van Gunsteren WF et al (1984) Molecular dynamics with coupling to an external bath. J Chem Phys 81(8):3684–3690. https://doi.org/10.1063/1.448118

Burgert I, Frühmann K, Keckes J et al (2004) Structure-function relationships of four compression wood types: micromechanical properties at the tissue and fibre level. Trees 18(4):480. https://doi.org/10.1007/s00468-004-0334-y

Bussi G, Donadio D, Parrinello M (2007) Canonical sampling through velocity rescaling. J Chem Phys 126(1):014101. https://doi.org/10.1063/1.2408420

Chen P, Wohlert J, Berglund L et al (2022) Water as an intrinsic structural element in cellulose fibril aggregates. J Phys Chem Lett 13(24):5424–5430. https://doi.org/10.1021/acs.jpclett.2c00781

Darden T, York D, Pedersen L (1993) Particle mesh ewald: an n·log(n) method for ewald sums in large systems. J Chem Phys 98(12):10089–10092. https://doi.org/10.1063/1.464397

Donaldson LA, Adya P. Singh (2016) Chapter 6 - Reaction Wood. In: Yoon Soo Kim, Ryo Funada, Adya P. Singh (eds) Secondary Xylem Biology. Academic Press, pp 93–110

Färber J, Lichtenegger HC, Reiterer A et al (2001) Cellulose microfibril angles in a spruce branch and mechanical implications. J Mater Sci 36:5087–5092. https://doi.org/10.1023/A:1012465005607

Fengel D (1971) Ideas on the ultrastructural organization of the cell wall components. J Polym Sci Part C: Polym Symp 36(1):383–392. https://doi.org/10.1002/polc.5070360127

Fernando D, Kowalczyk M, Guindos P et al (2023) Electron tomography unravels new insights into fiber cell wall nanostructure; exploring 3d macromolecular biopolymeric nano-architecture of spruce fiber secondary walls. Scientific Rep 13:2350. https://doi.org/10.1038/s41598-023-29113-x

Gardiner B, Barnett J, Saranpää P, et al (eds) (2014a) The Biology of Reaction Wood. Springer Series in Wood Science, Springer Berlin Heidelberg, Berlin, Heidelberg, https://doi.org/10.1007/978-3-642-10814-3

Gardiner B, Barnett J, Saranpää P, et al (eds) (2014b) Morphology, Anatomy and Ultrastructure of Reaction Wood, Springer Berlin Heidelberg, Berlin, Heidelberg, pp 13–35. https://doi.org/10.1007/978-3-642-10814-3_2,

Gibson LJ (2012) The hierarchical structure and mechanics of plant materials. J R Soc Interface 9:2749–2766. https://doi.org/10.1098/rsif.2012.0341

Gurau L, Cionca M, Mansfield-Williams H et al (2008) Comparison of the mechanical properties of branch and stem wood for three species. Wood Fiber Sci 40(4):647–656

Hackenstrass K, Hasani M, Wohlert M (2024) Structure, flexibility and hydration properties of lignin dimers studied with molecular dynamics simulations. Holzforschung. https://doi.org/10.1515/hf-2023-0054

Harris JM (1977) Shrinkage and density of radiata pine compression wood in relation to its anatomy and mode of formation. New Zealand J For Sci 7(1):16

Hartwig-Nair M, Florisson S, Wohlert M et al (2024) Characterisation of hygroelastic properties of compression and opposite wood found in branches of norway spruce. Wood Sci Technol. 58(3):887–906. https://doi.org/10.1007/s00226-024-01548-z

Hartwig-Nair M, Gamstedt EK, Florisson S et al (2024) Softwood branches modelled as a composite beam of compression and opposite wood: investigation of bending resistance. Wood Mater Sci Eng 19:1–8. https://doi.org/10.1080/17480272.2024.2365784

He H, Zhang C, Zhao X et al (2018) Allometric biomass equations for 12 tree species in coniferous and broadleaved mixed forests. Northeastern China. PLOS ONE 13(1):e0186226. https://doi.org/10.1371/journal.pone.0186226

Hockney R, Goel S, Eastwood J (1974) Quiet high-resolution computer models of a plasma. J Comput Phys 14(2):148–158. https://doi.org/10.1016/0021-9991(74)90010-2

Humphrey W, Dalke A, Schulten K (1996) Vmd: visual molecular dynamics. J Mol Graph 14(1):33–38

Inc. TM (2024) Matlab version: 24.2.0.2712019 (r2024b). URL https://www.mathworks.com

Joffre T, Neagu RC, Bardage SL et al (2014) Modelling of the hygroelastic behaviour of normal and compression wood tracheids. J Struct Biol 185(1):89–98. https://doi.org/10.1016/j.jsb.2013.10.014

Jorgensen WL, Chandrasekhar J, Madura JD et al (1983) Comparison of simple potential functions for simulating liquid water. J Chem Phys 79(2):926–935. https://doi.org/10.1063/1.445869

Kulasinski K, Guyer R, Derome D et al (2015) Water adsorption in wood microfibril-hemicellulose system: role of the crystalline-amorphous interface. Biomacromolecules 16:2972–2978. https://doi.org/10.1021/acs.biomac.5b00878

Kumar H, Dasgupta C, Maiti PK (2015) Structure, dynamics and thermodynamics of single-file water under confinement: effects of polarizability of water molecules. RSC Adv 5:1893–1901. https://doi.org/10.1039/C4RA08730E

Leonardon M, Altaner CM, Vihermaa L et al (2010) Wood shrinkage: Influence of anatomy, cell wall architecture, chemical composition and cambial age. Eur J Wood Prod 68(1):87–94. https://doi.org/10.1007/s00107-009-0355-8

Li X, Evans R, Gapare W et al (2014) Characterizing compression wood formed in radiata pine branches. IAWA J 35(4):385–394. https://doi.org/10.1163/22941932-00000073

Michaud-Agrawal N, Denning EJ, Woolf TB et al (2011) Mdanalysis: a toolkit for the analysis of molecular dynamics simulations. J Comput Chem 32(10):2319–2327. https://doi.org/10.1002/jcc.21787

Müller U, Gindl W, Jeronimidis G (2006) Biomechanics of a branch - stem junction in softwood. Trees 20(5):643–648. https://doi.org/10.1007/s00468-006-0079-x

Paajanen A, Zitting A, Rautkari L et al (2022) Nanoscale mechanism of moisture-induced swelling in wood microfibril bundles. Nano Lett 22(13):5143–5150. https://doi.org/10.1021/acs.nanolett.2c00822. (**pMID: 35767745**)

Páll S, Abraham MJ, Kutzner C et al (2015) Tackling exascale software challenges in molecular dynamics simulations with GROMACS. In: Markidis S, Laure E (eds) Solving Softw Chall Exascale. Springer International Publishing, Cham, pp 3–27

Perstorper M, Johansson M, Kliger R et al (2001) Distortion of Norway spruce timber. Holz Roh- Werkst 59:94–103. https://doi.org/10.1007/s001070050481

Ribca I, Sochor B, Roth SV et al (2023) Effect of molecular organization on the properties of fractionated lignin-based thiol-ene thermoset materials. Acs Omega 8(28):25478–25486

Stanzl-Tschegg SE, Keunecke D, Tschegg EK (2011) Fracture tolerance of reaction wood (yew and spruce wood in the TR crack propagation system). J Mech Behav Biomed Mater 4(5):688–698. https://doi.org/10.1016/j.jmbbm.2010.11.010

Timell TE (1986) Compress Wood Gymnosperms, 1st edn. Springer-Verlag, Berlin Heidelberg

Vermaas JV, Hardy DJ, Stone JE et al (2016) Topogromacs: automated topology conversion from charmm to gromacs within vmd. J Chem Inf Model 56(6):1112–1116

Vermaas JV, Petridis L, Ralph J et al (2019) Systematic parameterization of lignin for the charmm force field. Green Chem 21:109–122. https://doi.org/10.1039/C8GC03209B

Wohlert M, Benselfelt T, Wågberg L et al (2022) Cellulose and the role of hydrogen bonds: not in charge of everything. Cellulose 29(1):1–23. https://doi.org/10.1007/s10570-021-04325-4

Zhang M, Chavan RR, Smith BG et al (2016) Tracheid cell-wall structures and locations of (1 → 4)-β-d-galactans and (1 → 3)-β-d-glucans in compression woods of radiata pine (Pinus radiata D. Don). BMC Plant Biology 16(1):194. https://doi.org/10.1186/s12870-016-0884-3

Zhang C, Chen M, Sinan Keten BC et al (2021) Hygromechanical mechanisms of wood cell wall revealed by molecular modeling and mixture rule analysis. Sci Adv 7(37):eabi8919

Zitting A, Paajanen A, Penttilä PA (2023) Impact of hemicelluloses and crystal size on x-ray scattering from atomistic models of cellulose microfibrils. Cellulose 30(13):8107–8126. https://doi.org/10.1007/s10570-023-05357-8

Publisher's Note Springer Nature remains neutral with regard to jurisdictional claims in published maps and institutional affiliations.

Authors and Affiliations

Marie Hartwig-Nair[1] · Alexandr Nasedkin[1] · Klara Hackenstrass[1] · Emiliano De Santis[2] · Sara Florisson[1] · Malin Wohlert[1]

✉ Malin Wohlert
malin.wohlert@angstrom.uu.se

Marie Hartwig-Nair
marie.hartwig@angstrom.uu.se

Alexandr Nasedkin
alexnasedkin@gmail.com

Klara Hackenstrass
klara.hackenstrass@angstrom.uu.se

Emiliano De Santis
edesantis@roma2.infn.it

Sara Florisson
sara.florisson@angstrom.uu.se

[1] Applied Mechanics, Department of Materials Science and Engineering, Uppsala University, Box 35, 75103 Uppsala, Sweden

[2] Department of Physics and INFN, University of Rome Tor Vergata, via della Ricerca Scientifica 1, 00133 Rome, Italy